ICAS 2021 SHANG HAI
International Council of the Aeronautical Sciences
32nd Congress of the International Council of the Aeronautical Sciences
September 6-10, 2021 Pudong Shangri-La, Shanghai, China

# AN ADJOINT-BASED AERO-STRUCTURAL DESIGN OPTIMIZATION METHOD USING DYNAMIC MESH TECHNOLOGY

Jingrui Guo[1], Yi Li[2], Min Xu[1]

[1]School of Astronautics, Northwestern Polytechnical University, Xi'an 710072, Shaanxi, P.R.China
[2]School of Aeronautics, Northwestern Polytechnical University, Xi'an 710072, Shaanxi, P.R.China

## Abstract

Under the influence of aerodynamics and structure, an adjoint-based aero-structural coupling optimization approach is built to solve the jig-shape design problem in this paper. In this approach, Euler solver, FEM solver and dynamic mesh technology are used to make up the aero-structural coupling analysis solver. At the same time, an optimization case is given to demonstrate this methodology. For this optimization problem, the objective is to improve the lift-to-drag ratio of a subsonic wing, the independent variables are the geometric control parameter and structural sizes, and the main constraints are structural stress constraint and maximum mass change constraints. After optimization, the lift-to-drag ratio of the subsonic wing is improved from 33.503 to 37.333, the mass is reduced by 18.315%, and all structural stress constraints are satisfied. Therefore, the coupling optimization method is effective.

**Keywords:** aero-structural, adjoint, coupling optimization

## 1. Introduction

Jig-shape design of the aircraft is a complex problem, and performance of the final case is largely influenced by multiple disciplines such as aerodynamics and structure. At the same time, the traditional design method doesn't consider the relationship between disciplines at all stages, so it's hard to fully consider the influence of multidisciplinary coupling effect in the final scheme. Therefore, we need a new coupling optimization method to introduce the coupling effect into the design process. However, the cost of aero-structural coupling analysis approach decides that simply combining optimization algorithm and coupling analysis method is hard to accept. Therefore, based on the adjoint approach and the dynamic mesh technology, an aero-structural coupling optimization approach is built.

Several aero-structural analysis models have been built to deal with the aero-structural coupling problem [1]. For adjoint approach, at the same time, in the field of optimization, active research work based on this approach was achieved. An aero-structural coupling optimization methodology was developed by Joaquim Martins, and this method is used to design the jig shape of subsonic wing [2,3]. Nicolas R. Gauger developed a kind of continuous adjoint approach which was used to solve the aerodynamic shape optimization problem [4]. In the field of high-fidelity aero-structural coupling analysis, two gradient computation methods for design variables were presented by Timothee Achard [5]. And, some work was done for supersonic wings [6].

This paper is divided into three parts: methodology, optimization case and conclusions. In the first part, the aero-structural coupling analysis approach is introduced, and the details about coupling analysis solver, adjoint approach and optimization approach are given. In the second part, a case of aero-structural coupling optimization is given, whose objective function is lift-to-drag ratio and independent variables are structural size and geometric control parameter. In the last part, conclusions and discussion of this paper are given.

## 2. Methodology

### 2.1 Overview

The coupling optimization method includes three aspects: Coupling analysis solver, Adjoint approach

and Optimization approach. The details of the three aspects are given in the Section 2.2 to Section 2.4. All steps of the coupling optimization method are given in Figure 1. Firstly, the design parameters (expressed by $\mathrm{p}$) including the geometric control parameter are transformed into the form which can be recognized by the coupling optimization solver, and the details of this part are given in Section 2.4. Secondly, the aero-structural coupling analysis model is used for the coupling analysis of the wing, and the parameters required by the optimization approach (e.g., objective function $\mathrm{I}$) and adjoint approach are also calculated. It can be found that the aero-structural coupling analysis solver is built up by the CFD solver and the FEM solver, and all the details of this coupling analysis solver are given in Section 2.2. Thirdly, the gradient information (e.g., $\mathrm{dI/dp}$) is calculated by the adjoint approach, and the results of this step are required by the optimization. In Section 2.3, the details of the adjoint approach are given. Finally, based on the gradient information and the objective function, the optimization approach gives us the new design parameters, and the details are also given in the Section 2.4.

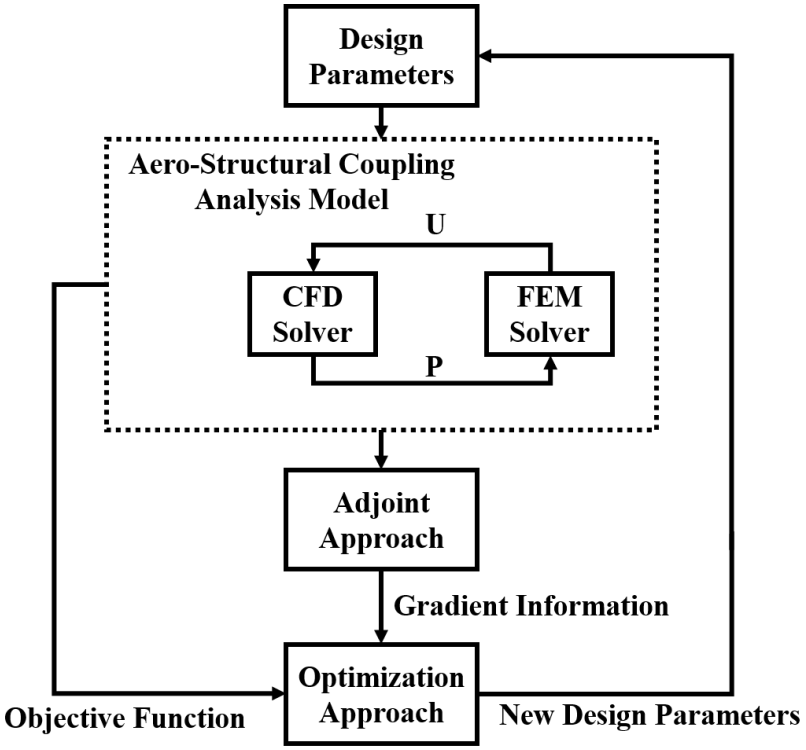


Figure 1 – Schematic diagram of the coupling optimization method

## 2.2 Coupling Analysis Solver

In this Section, the details of the aero-structural coupling analysis solver are given, and the schematic diagram of the areo-structural coupling analysis solver is given in Figure 2. It can be found that the coupling analysis solver is mainly composed of CFD solver, FEM solver and compactly support radial basis function approach (CS-RBF). $\boldsymbol{P_a}$ and $\boldsymbol{U_a}$ are the pressure and displacement based on the Surface grid nodes of aerodynamic mesh. $\boldsymbol{P_s}$ and $\boldsymbol{U_s}$ are the pressure and displacement based on the Surface grid nodes of structural mesh.

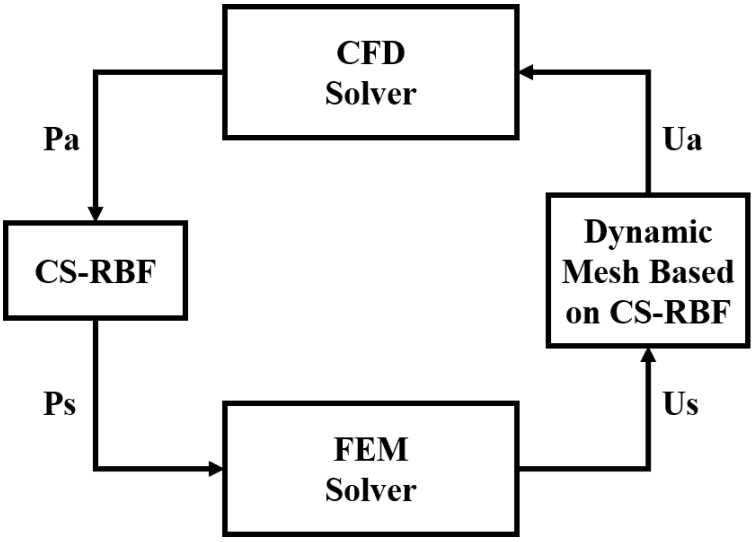


Figure 2 – Schematic diagram of the coupling analysis solver

Euler solver of the open-source code SU2 is used in our work as the CFD solver, which is a finite-volume CFD solver for the unstructured meshes. At the same time, the flow state variable $\boldsymbol{w_a}$ can be represented by the variable $\boldsymbol{Q}$, which can be written as Equation (1).

$$\boldsymbol{Q} = \begin{bmatrix} \rho \\ \rho v_x \\ \rho v_y \\ \rho v_z \\ \rho e \end{bmatrix} \tag{1}$$

For the three-dimensional problems, $\rho$ is the density of the fluid, and e is the total energy per unit mass of the fluid. $v_x$, $v_y$ and $v_z$ are the velocities of the fluid in three directions. Based on the flow state variable w, the pressure distribution P can be calculated.

MSC. Nastran is used in our work as the CSD solver. Beam elements, shell elements and rod elements are all used to construct the finite element model, and the finite element model of the wing can be divided into three parts: rib, spar and skin. For the rib part, as the figure 3, the structure is made up by the flange and the web, the flange is simulated by the rod elements, and the web is simulated by the shell elements.

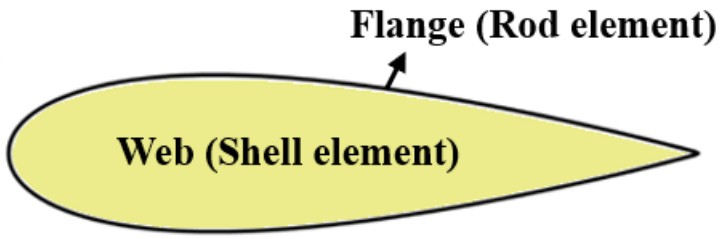


Figure 3 – Rib of the wing

For the spar part, as the figure 4, the structure is also made up by the flange and the web, the web is also simulated by the shell elements, but the flange is simulated by the beam elements.

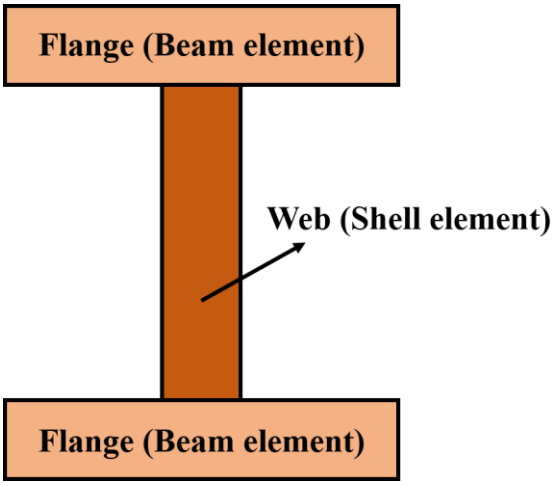


Figure 4 – Spar of the wing

For the skin part, the structure is only simulated by the shell elements. At the same time, the structure state variable $\boldsymbol{w_s}$ is the displacement of structural grid nodes, which is used in the next section.

At the same time, we also need an interpolation algorithm to deal with the data transfer problem between structural mesh and aerodynamic mesh, and CS-RBF [7] is selected in this paper. For three-dimensional problems, the basis function of CS-RBF used in this paper is $C^2$, and the its expression is shown as Equation (2).

$$\phi(r) = \begin{cases} (1-r)^4(4r+1) & 0 \le r \le 1 \\ 0 & r > 1 \end{cases} \quad r = \frac{\|x - x_0\|}{r_0} \tag{2}$$

## 2.3 Adjoint Approach

Adjoint approach can get the gradient information efficiently. The details of this approach used in the aero-structural coupling analysis is given in the paper of Martins [2]. In this section, the equation of the adjoint approach used in this paper is given.

Firstly, for aero-structural coupling optimization problem, the gradient information can be written as Equation (3).

$$\frac{dI}{d\boldsymbol{p}} = \frac{\partial I}{\partial \boldsymbol{p}} + \frac{\partial I}{\partial \boldsymbol{w_a}}\frac{\partial \boldsymbol{w_a}}{\partial \boldsymbol{p}} + \frac{\partial I}{\partial \boldsymbol{w_s}}\frac{\partial \boldsymbol{w_s}}{\partial \boldsymbol{p}} \tag{3}$$

For the aerodynamic governing equations ($S_a$) and the structural governing equations ($S_s$) the total derivatives are equal to zero.

$$\begin{aligned} \frac{d\boldsymbol{S_a}}{d\boldsymbol{p}} &= \frac{\partial \boldsymbol{S_a}}{\partial \boldsymbol{p}} + \frac{\partial \boldsymbol{S_a}}{\partial \boldsymbol{w_a}}\frac{\partial \boldsymbol{w_a}}{\partial \boldsymbol{p}} + \frac{\partial \boldsymbol{S_a}}{\partial \boldsymbol{w_s}}\frac{\partial \boldsymbol{w_s}}{\partial \boldsymbol{p}} = 0 \\ \frac{d\boldsymbol{S_s}}{d\boldsymbol{p}} &= \frac{\partial \boldsymbol{S_s}}{\partial \boldsymbol{p}} + \frac{\partial \boldsymbol{S_s}}{\partial \boldsymbol{w_a}}\frac{\partial \boldsymbol{w_a}}{\partial \boldsymbol{p}} + \frac{\partial \boldsymbol{S_s}}{\partial \boldsymbol{w_s}}\frac{\partial \boldsymbol{w_s}}{\partial \boldsymbol{p}} = 0 \end{aligned} \tag{4}$$

Based on the adjoint vectors ($\boldsymbol{\varphi_a}, \boldsymbol{\varphi_s}$), Equation (3) and Equation (4), the Equation (5) is given.

$$\begin{aligned} \frac{dI}{d\boldsymbol{p}} = \frac{\partial I}{\partial \boldsymbol{p}} + \frac{\partial I}{\partial \boldsymbol{w_a}}\frac{d\boldsymbol{w_a}}{d\boldsymbol{p}} + \frac{\partial I}{\partial \boldsymbol{w_s}}\frac{d\boldsymbol{w_s}}{d\boldsymbol{p}} + \boldsymbol{\varphi_a}\left(\frac{\partial \boldsymbol{S_a}}{\partial \boldsymbol{p}} + \frac{\partial \boldsymbol{S_a}}{\partial \boldsymbol{w_a}}\frac{\partial \boldsymbol{w_a}}{\partial \boldsymbol{p}} + \frac{\partial \boldsymbol{S_a}}{\partial \boldsymbol{w_s}}\frac{\partial \boldsymbol{w_s}}{\partial \boldsymbol{p}}\right) \\ + \boldsymbol{\varphi_s}\left(\frac{\partial \boldsymbol{S_s}}{\partial \boldsymbol{p}} + \frac{\partial \boldsymbol{S_s}}{\partial \boldsymbol{w_a}}\frac{\partial \boldsymbol{w_a}}{\partial \boldsymbol{p}} + \frac{\partial \boldsymbol{S_s}}{\partial \boldsymbol{w_s}}\frac{\partial \boldsymbol{w_s}}{\partial \boldsymbol{p}}\right) \end{aligned} \tag{5}$$

The Equation (5) can be rewritten as Equation (6).

$$\begin{aligned} \frac{dI}{d\boldsymbol{p}} = \frac{\partial I}{\partial \boldsymbol{p}} + \boldsymbol{\varphi_a}\frac{\partial \boldsymbol{S_a}}{\partial \boldsymbol{p}} + \boldsymbol{\varphi_s}\frac{\partial \boldsymbol{S_s}}{\partial \boldsymbol{p}} + \left(\frac{\partial I}{\partial \boldsymbol{w_a}} + \boldsymbol{\varphi_a}\frac{\partial \boldsymbol{S_a}}{\partial \boldsymbol{w_a}} + \boldsymbol{\varphi_s}\frac{\partial \boldsymbol{S_s}}{\partial \boldsymbol{w_a}}\right)\frac{d\boldsymbol{w_a}}{d\boldsymbol{p}} \\ + \left(\frac{\partial I}{\partial \boldsymbol{w_s}} + \boldsymbol{\varphi_a}\frac{\partial \boldsymbol{S_a}}{\partial \boldsymbol{w_s}} + \boldsymbol{\varphi_s}\frac{\partial \boldsymbol{S_s}}{\partial \boldsymbol{w_s}}\right)\frac{\partial \boldsymbol{w_s}}{\partial \boldsymbol{p}} \end{aligned} \tag{6}$$

$\boldsymbol{\varphi_a}$ and $\boldsymbol{\varphi_s}$ can be calculated by the Equation (7).

$$\begin{pmatrix} \frac{\partial S_a}{\partial w_a}^T & \frac{\partial S_s}{\partial w_a}^T \\ \frac{\partial S_a}{\partial w_s}^T & \frac{\partial S_s}{\partial w_s}^T \end{pmatrix} \begin{pmatrix} \boldsymbol{\varphi_a} \\ \boldsymbol{\varphi_s} \end{pmatrix} = \begin{pmatrix} -\frac{\partial I}{\partial w_a} \\ -\frac{\partial I}{\partial w_s} \end{pmatrix} \tag{7}$$

Finally, the gradient information can be calculated by the Equation (8).

$$\frac{dI}{d\boldsymbol{p}} = \frac{\partial I}{\partial \boldsymbol{p}} + \boldsymbol{\varphi_a} \frac{\partial S_a}{\partial \boldsymbol{p}} + \boldsymbol{\varphi_s} \frac{\partial S_s}{\partial \boldsymbol{p}} \tag{8}$$

## 2.4 Optimization Approach

Based on the actual design process, we divide the wing design into the static strength design stage (based on the 2.5g load condition) and the cruise design stage (based on the 1g load condition). And in this paper, the cruise design stage is what we need to consider, and result of the static strength design stage is only used as the initial value of the next stage.

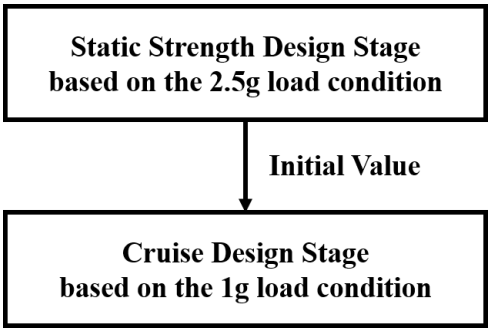


Figure 5 – Schematic diagram of the design

Since the optimization problem can be approximated as a continuous problem, we used the optimization algorithm based on the internal penalty function method [8] to solve the problem, and the schematic diagram is given in figure 6.

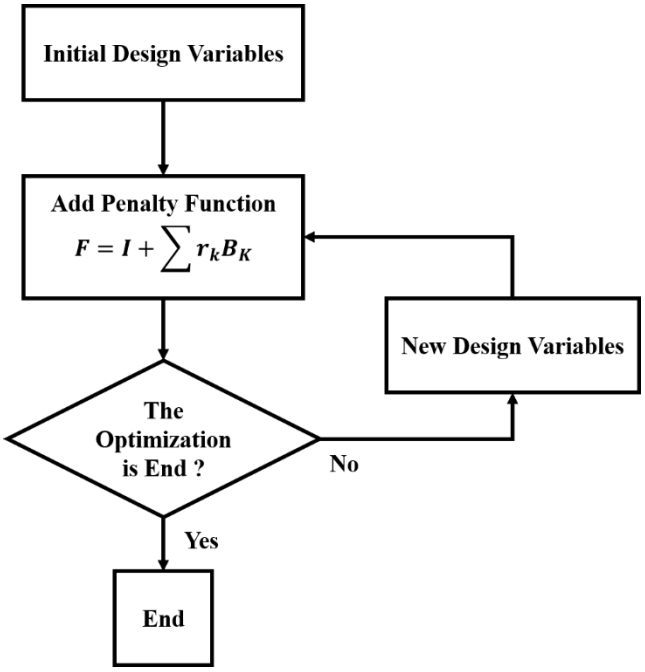


Figure 5 – Schematic diagram of the optimization algorithm

At the same time, due to the complexity of the wing structure, induced exponential aggregation [9] is used to deal with the constraint, and the induced exponential functional is given by Equation (9).

$$C_{IE}(c,\rho)=\frac{\int_{\Omega}\frac{c}{c_{aim}}e^{\rho\frac{c}{c_{aim}}}d\Omega}{\int_{\Omega}e^{\rho\frac{c}{c_{aim}}}d\Omega} \tag{9}$$

When $c < c_{aim}$ is satisfied, $C_{IE}$ is less than 1. At the same time, $C_{IE}$ is greater than 1, when $c > c_{aim}$ is not satisfied.

In addition, at the beginning of the optimization approach, it is necessary to parameterize the geometry. In this paper, geometry is only decided by the geometric control parameter ($\alpha$) and the initial geometry. It is assumed that the geometric twist angles of the optimized wing change linearly along the span rectangle. So, the geometric twist angle can be calculated by Equation (10). $L_{wing}$ is the half wing span, and $l$ is the position of the point.

$$\theta=\alpha\frac{l}{L_{wing}} \tag{10}$$

In Figure 6, an example of the geometric control parameter used to control the geometric shape is shown, and in order to show more clearly $\alpha = 20$ which is too large for our optimization.

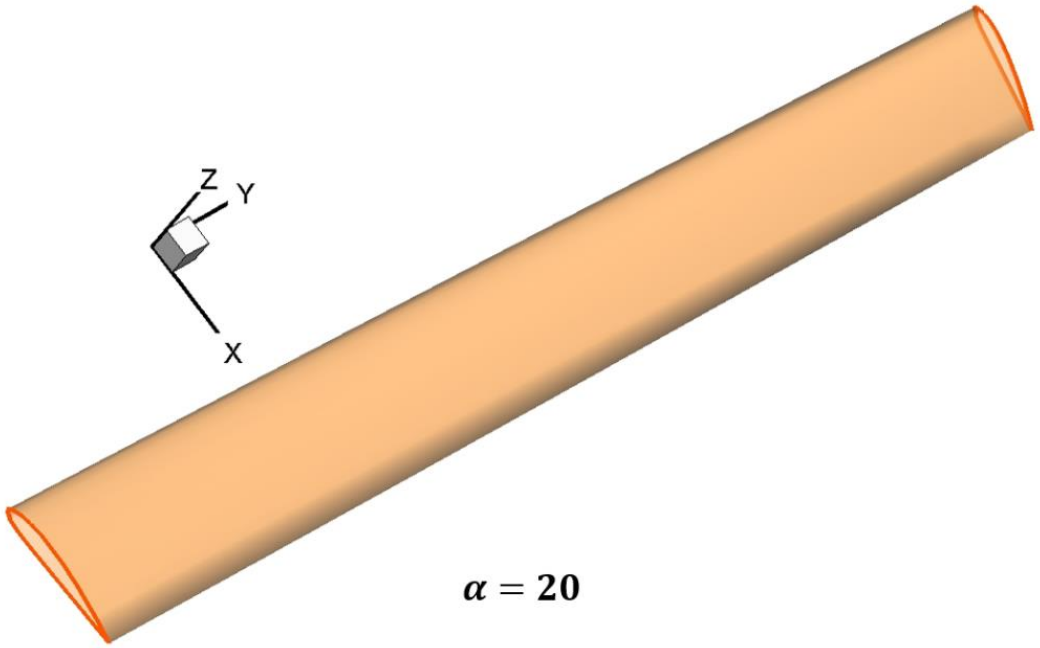


Figure 6 –Wing geometry controlled by the geometric control parameter

## 3. Optimization Case

### 3.1 Optimization Problem

In this section, an aero-structural coupling optimization problem is given to show the optimization approach described in section 2.1 to section 2.4. The optimization object of this coupling optimization problem is a wing, and the details of the wing is given in figure 7.

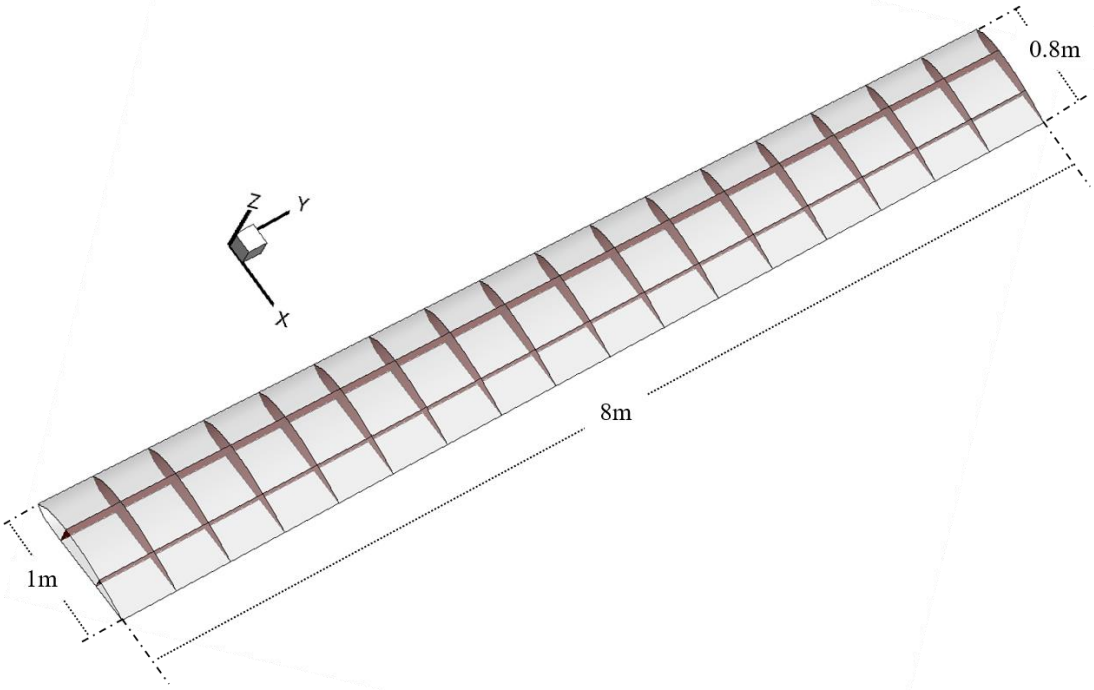


Figure 7 –Details of the wing

At the same time, the basic geometric parameters of the wing are given in Table 1.

Table 1 Geometric parameters of the wing

| Parameters | Values |
|---|---|
| Half span | 8m |
| Leading edge sweep | 14.48° |
| Root chord length | 1m |
| Taper ratio | 0.8 |
| Airfoil | NACA4415 |
| Number of ribs | 17 |
| Number of spars | 2 |
| Location of spars | 0.3, 0.7 |

As shown in Table 1, half span of the wing is 8m and leading-edge sweep is 14.48°. Root chord length is 1m, and taper ratio is 0.8. Seventeen wing ribs are distributed uniformly along span. Chord positions of the two spars are 30% and 70% respectively.

Table 2 Cruise conditions of the aerodynamic cases

| Parameters | Values |
|---|---|
| Mach Number | 0.3 |
| Attack Angle | 5° |
| Freestream pressure | $101325Pa$ |
| Reference Length | $8.0m$ |
| Reference Area | $7.2m^2$ |

The wing is to fly at Mach 0.3 and the airfoil is NACA4415. Cruise conditions (1g load condition) of the wing are given in the Table 2. Based on the basic geometric parameters, the aerodynamic grid used in this work is shown in Figure 8.

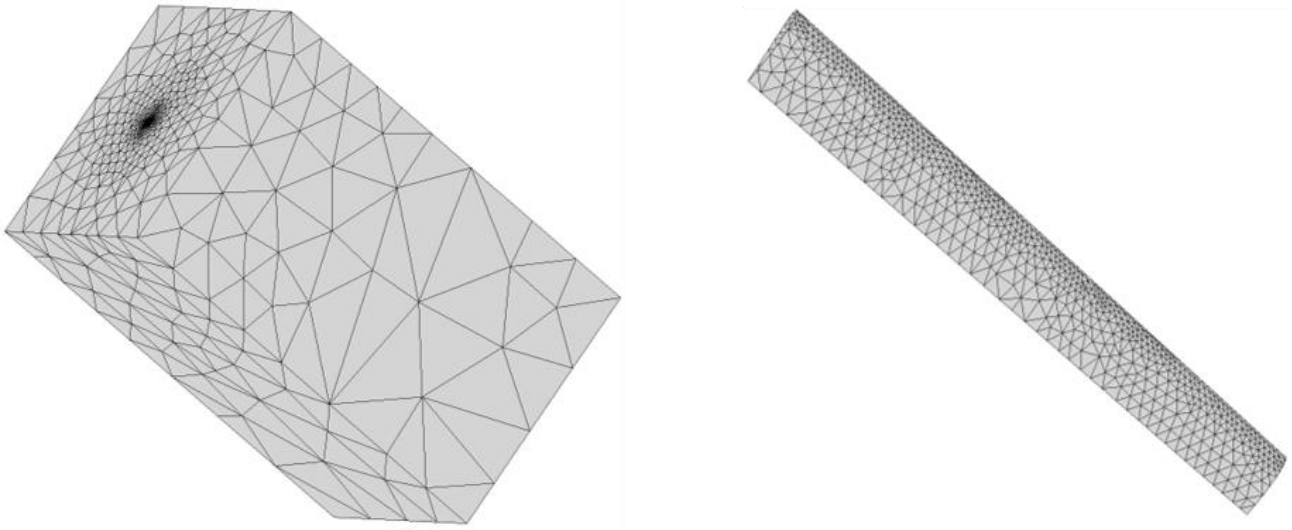

(a) (b)

Figure 8 – Aerodynamic grid of the wing

In this section, the objective of the coupling optimization problem is to maximize the lift-drag ratio of the wing. The design variables include structural sizes and geometric control parameter, and the main constraint of this problem is structural stress constraint, maximum mass change constraints and structural sizes constraint. Overview of the optimization problem is given in Table 3.

Table 3 Overview of the Optimization Problem

| | Function/Variable | Description |
|---|---|---|
| maximize | $\frac{C_l}{C_d}$ | Lift-drag Ratio |
| w.r.t | $t_{size}$ | structural sizes (Excluding the Cross-sectional Area of Rod) |
| | $\alpha$ | Geometric Control Parameter |
| Subject to | $\sigma_{max} \leq 350\text{MPa}$ | Maximum Equivalent Stress is Less Than the Yield Strength of Material (350MPa) |
| | $\Delta M_{wing} \leq 20\%$ | The change of the mass is less than $20\%$ |
| | $L - M_{all} \leq 5\%$ | 1g Load Constraint |
| | $S_a = 0$ | Aerodynamic Governing Equations |
| | $S_s = 0$ | Structural Governing Equations |

## 3.2 Results and Discussion

In this section, for the optimization case described in Section 3.1, the initial case, optimal case and related discussion are given. It should be noted that only cruise design stage is involved in this section.

In Figure 9, for the thicknesses of skin, the initial and optimal values are given. The thicknesses of lower skin are given in the upper part of this figure, and the ones of upper skin are given in the lower part.

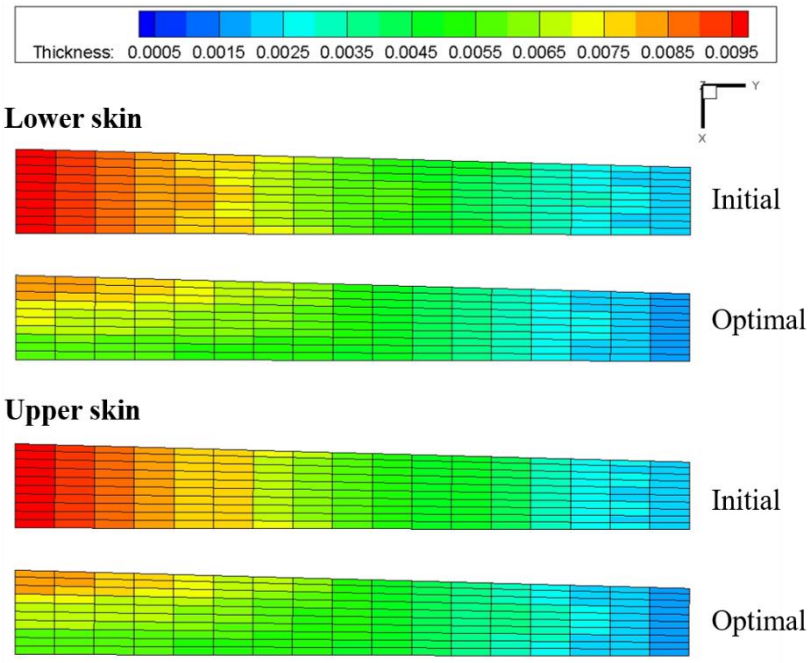


Figure 9 – Thicknesses of skin

In Figure 10, for web of spar and rib, the initial and optimal thicknesses are given. The initial thicknesses are given in the upper part of this figure, and the optimal ones are given in the lower part.

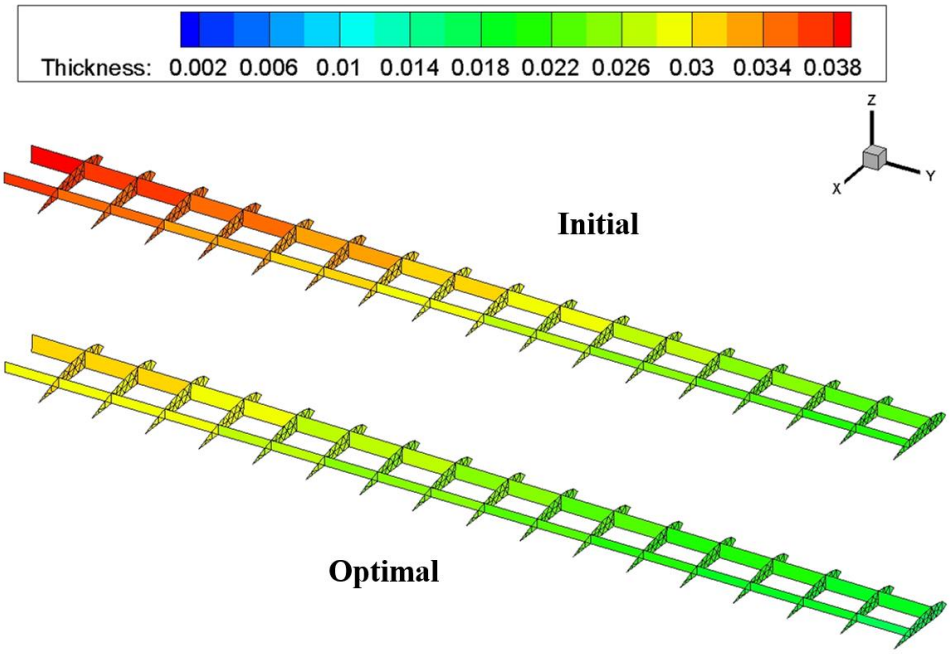


Figure 10 – Thicknesses of web of spar

In Figure 11, for flange of spar, the initial and optimal sizes are given. The widths of the beam elements are given in the upper part of this figure, and the highs of the beam elements are given in the lower part.

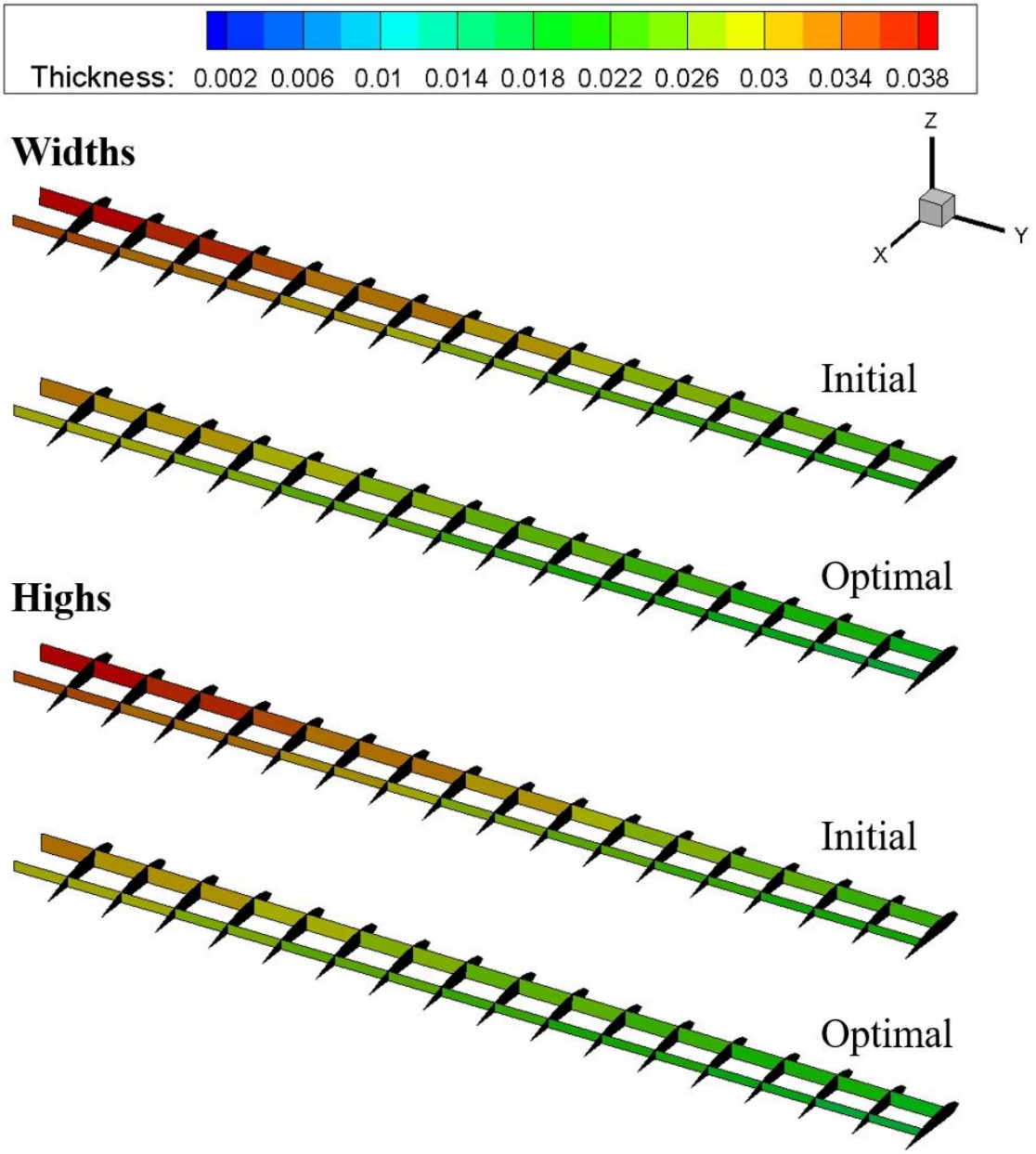


Figure 11 – Sizes of flange of spar

For geometric control parameter, the initial value is 1, and the optimal value is 0.291. Based on Figure 9, Figure10 and Figure 11, it can be found that most of the structural sizes are reduced, which may be caused by the 1g load constraint. And, the change of the structural sizes leads to the change of mass, deformation and Von Mises stress. Mass of initial case is 649.378kg, and the one of optimal case is 530.444kg. Deformation and Von Mises stress of the initial and optimal case are given in Figure 12.

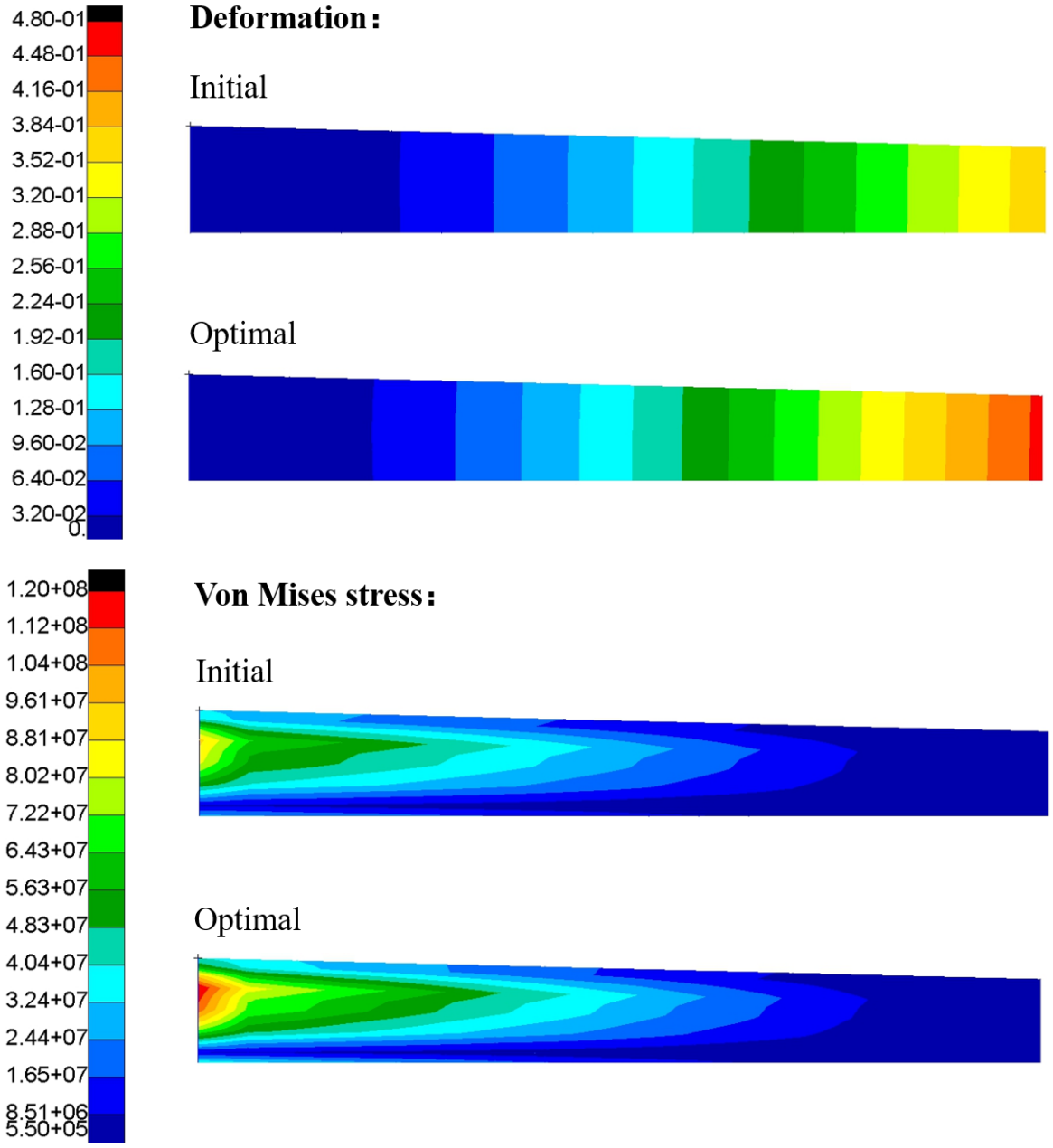


Figure 12 – Distribution of the deformation and Von Mises stress

Optimization history of the objective function is given in Figure 13, and lift-drag ratio increases from 33.503 to 37.333.

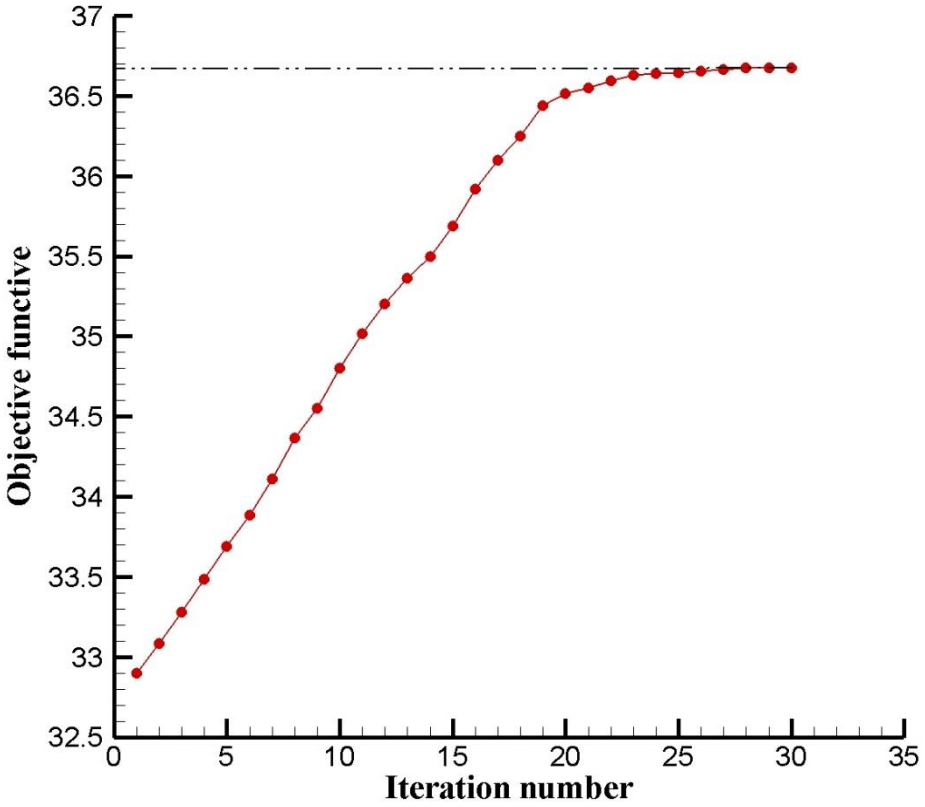


Figure 13 – Optimization history of the objective function

In conclusion, the optimization of structural sizes and geometric control parameter can effectively increase the lift-drag ratio. After optimization, lift-to-drag ratio increases from 33.503 to 37.333, mass of the wing reduces from 649.1945kg to 530.444kg, and all stress constraints are satisfied.

## 4. Conclusions

In this paper, in order to solve the jig-shape design problem, based on the aero-structural analysis solver and adjoint approach, a coupling optimization approach is built. And, the design case of a subsonic wing is optimized by the coupling optimization approach. The objective is to improve the lift-to-drag ratio of the wing, and the design variables include geometric control parameter and structural sizes. After optimization, the lift-to-drag ratio of the subsonic wing is improved from 33.503 to 37.333. For structural stress constraints, the max stress is less than the yield strength of material (350MPa). For maximum mass change constraints, the mass is reduced from 649.378kg to 530.444kg, and the change is less than 20%. Therefore, effectiveness of the coupling optimization approach can be authenticated by this optimization case.

## 5. Contact Author Email Address

mailto: liyi504@nwpu.edu.cn

## 6. Copyright Statement



## References

[1] Mcnamara JJ, Friedmann PP. Aeroelastic and Aerothermoelastic Analysis in Hypersonic Flow: Past, Present, and Future. AIAA J. Vol. 49, No. 6, pp 1089-122, 2011.

[2] Martins JR, A coupled-adjoint method for high-fidelity aero-structural optimization. Dissertation, Stanford

University, 2002.

[3] Burdette DA, Martins JR Design of a transonic wing with an adaptive morphing trailing edge via aerostructural optimization. Aerospace Science and Technology. Vol. 81, pp 192-203, 2018.

[4] Gauger N. Adjoint approaches in aerodynamic shape optimization and MDO context. Eccomas Cfd DLR. 2006.

[5] Achard T, Blondeau C, Ohayon R. COMPARISON OF HIGH-FIDELITY AERO-STRUCTURE GRADIENT COMPUTATION TECHNIQUES. APPLICATION ON THE CRM WING DESIGN. IFASD 2017.

[6] Guo J, Li Y, Xu M, et al. Aero-structural optimization of supersonic wing under thermal environment using adjoint-based optimization algorithm. Structural and Multidisciplinary Optimization, 2021.

[7] Beckert A, Wendland H. Multivariate interpolation for fluid-structure-interaction problems using radial basis functions. Aerospace Science & Technology, Vol. 5, No. 2, pp 125-134, 2001.

[8] Du, X., Wang, H., Dang, Q., Liu, X., & Huang, Y. Optimization Algorithm of Initial Orbit Based on Internal Penalty Function Method. In: 2007 IEEE International Conference on Systems, Man and Cybernetics. IEEE, pp 3202-3207, 2007.

[9] Lambe AB, Kennedy GJ, Martins JR. An evaluation of constraint aggregation strategies for wing box mass minimization. Struct Multidiscip Optim, Vol. 55, No. 1, pp 257-277, 2017.